RFPD Topology Comparison
LIGO-T060268-00-C
R. Abbott, Caltech
6 November, 2006

1. Overview

Several different topologies of RFPD design are analyzed from the standpoint of signal-to- noise ratio (SNR), and topological advantages.

1.1. The shot noise resulting from DC photo-current flowing in the diode is treated as the "signal" during the analysis.

1.2. The "noise" term results from the voltage and current noise intrinsic to RF amplifier that processes the signal from the diode. Other noise terms are not considered for this analysis.

1.3. For the purpose of numerical comparison the following standard conditions are assumed:

- Analysis Frequency = 50 MHz
- Input referred voltage noise of op-amp = 2nV/√Hz
- Input referred current noise of op-amp = 3pA/√Hz
- DC Photocurrent = 50mA
- RF transimpedance = 100Ω

2. Photodiode Model

The comparison of different photo-detector topologies uses a standard photo-diode model as shown in Figure 1. The constant-current source I1 represents the source of DC photocurrent. C1 is the diode capacitance; R1 is the diode series resistance element.

Figure 1

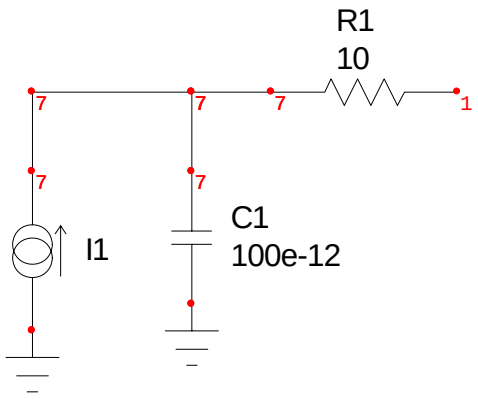

3. **Initial LIGO** topology with components for 50 MHz RF tank resonance and 100Ω RF transimpedance (at input to X_4).

Figure 2

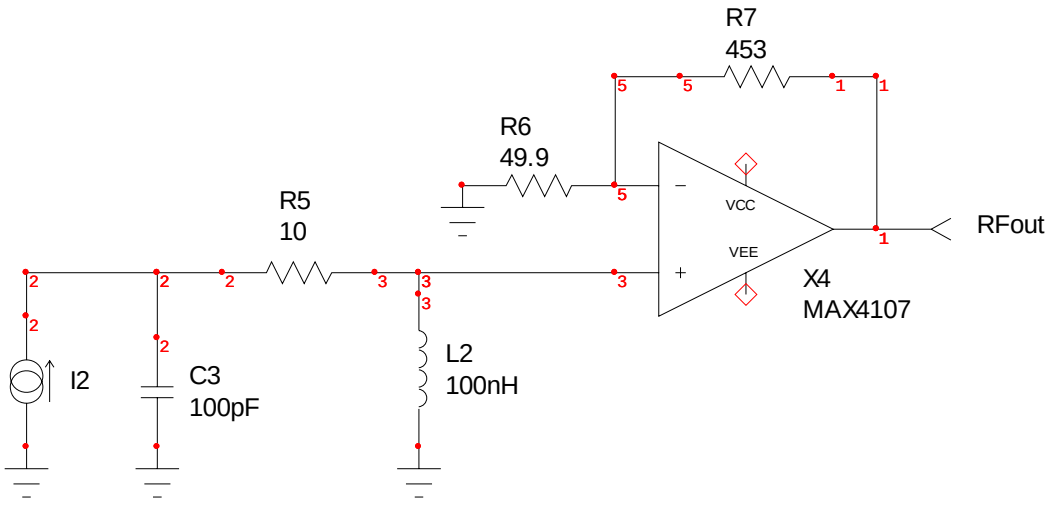

3.1. The signal voltage at the positive input to the op-amp is given by:

3.1.1. $V_{signal}=I_{shot}\cdot Z_{tank}$ where:

$I_{shot}=\sqrt{2\cdot e\cdot I_2}$

e is the electron charge of 1.602 e-19 coulombs

$Z_{tank}=\dfrac{L_2}{R_5\cdot C_3}$ (Only valid at resonance)

3.1.2. Substitution yields: $V_{signal}=\sqrt{2\cdot e\cdot I_2}\cdot\dfrac{L_2}{R_5\cdot C_3}$

3.2. The voltage noise at the input to the op-amp is expressed as:

3.2.1. $V_{noise}=\sqrt{(V_n)^2+(I_n\cdot Z_{tank})^2}$ where:

V_n and I_n are the input referred voltage and current noise spectral densities for the operational amplifier

3.3. The SNR (Signal-to-Noise Ratio) at the input to the op-amp is therefore:

3.3.1. $SNR=\dfrac{I_{shot}\cdot Z_{tank}}{\sqrt{(V_n)^2+(I_n\cdot Z_{tank})^2}}$

3.4. Using the formula for SNR and the standard initial conditions the calculated SNR is:

SNR = 6.25

As the signal and noise both experience the same amplification through the operational amplifier, the output SNR is (to first order) the same.

4. **Sandberg-GEO-Virgo Style Design.** The values of L_2 and C_4 have been adjusted for 100 Ω RF transimpedance at 50 MHz center frequency.

Figure 3

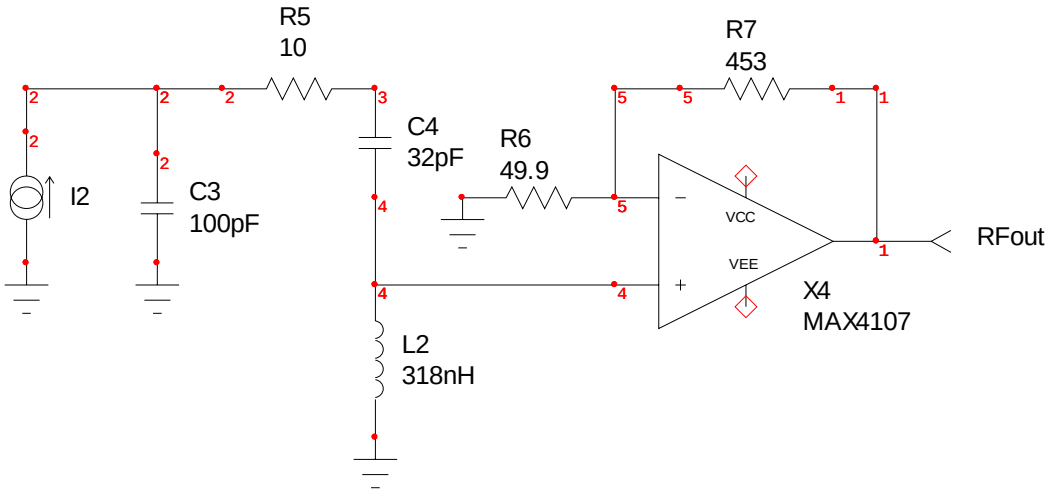

4.1. The signal voltage at the positive input to the op-amp at the resonance of C_4 and L_2 is given by:

4.1.1. $$V_{signal} = I_{shot} \cdot \omega \cdot L_2 \sqrt{\frac{1}{1+(\omega \cdot R_5 \cdot C_3)^2}}$$

4.2. Figure 4 shows the reactive elements of Figure 3, redrawn to emphasize the effect of op-amp input current noise. At the series resonant frequency (50MHz) of C_4 and L_2, the op-amp input noise current represented by I_{noise} will develop a corresponding noise voltage.

Figure 4

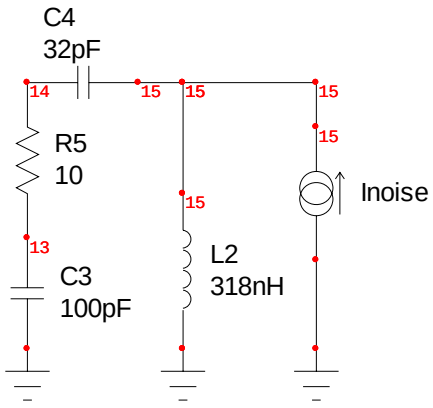

At 50MHz, this is no longer a resonant network, so the network impedance is slightly more complex.

4.2.1. The magnitude of the impedance presented by the network in Figure 4 can be calculated by:

$$Z_{network} = \sqrt{\frac{R_5^{\,2} + (\omega \cdot L_2)^2}{(1 - \omega^2 \cdot L_2 \cdot C)^2 + (\omega \cdot C \cdot R_5)^2}}$$

Where C is the series combination of C_4 and C_3

4.2.2. The resultant total noise (related to the op-amp input voltage and current noise) as seen at the positive input to the op-amp can now be calculated by:

$$V_{noise} = \sqrt{(V_n)^2 + (I_n \cdot Z_{network})^2}$$

4.2.3. Taking the ratio of the signal and noise voltages, the SNR is calculated to be:

SNR = 5.17

As the signal and noise both experience the same amplification through the operational amplifier, the output SNR is (to first order) the same.

5. **Variant 1**.

A topology is shown in Figure 5 using a transimpedance amplifier configuration to read current through a series resonator.

Figure 5

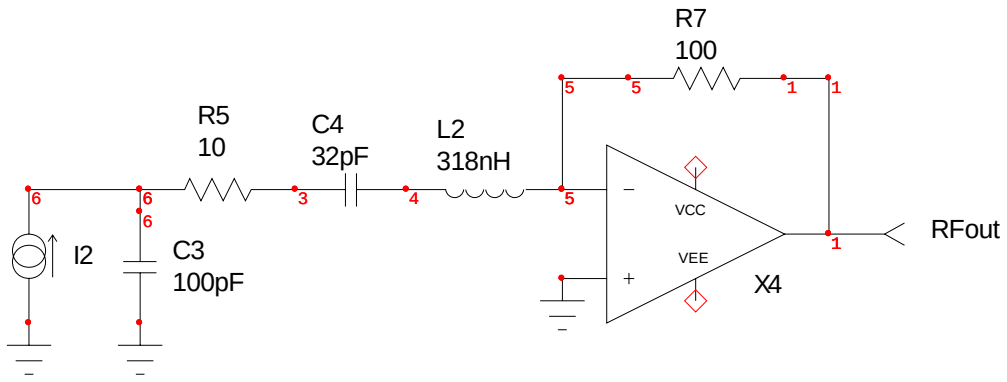

5.1. Assuming C_4 and L_2 are driven at their series resonant frequency ω, and any resistance associated with L_2 is absorbed in the value of R_5, and the op-amp X_4 has an open loop gain >>1 at ω, the magnitude of the current flowing through R_5 can be shown to equal:

$$I_{R5} = I_2 \cdot \sqrt{\frac{1}{1+(\omega \cdot R_5 \cdot C_3)^2}}$$

5.2. The RF transimpedance of this stage is 100 Ω, as set by R_7. A shot noise signal of the nominal level (50mA photocurrent) will result in a voltage at the RFout port expressed by:

$$Vsignal_{RFout} = I_{shot} \cdot R_7 \sqrt{\frac{1}{1+(\omega \cdot R_5 \cdot C_3)^2}}$$

5.3. The amplifier X_4 has an input impedance of <<1Ω provided the open loop gain is >>1 at the frequency of interest (50 MHz in this example). The amplifier is configured for a transimpedance of 100, and a voltage gain of 1. The noise voltage at the output of X_4 (neglecting the thermal noise of R_7) is calculated as:

$$V_{noise} = \sqrt{(V_n)^2 + (I_n \cdot R_7)^2}$$

Notice that the op-amp voltage noise experiences a gain of 1 through the amplifier

5.4. The **SNR** at the output of X_4 is calculated by the ratio of the output signal voltage to the output noise voltage using the nominal parameters:

SNR = 5.97

The improvement in SNR for this topology is a consequence of the op-amp voltage gain being unity, thus the op-amp voltage noise is not amplified.

5.5. A parasitic resonance formed by L_2, C_3 and C_4 causes a peak in the overall RF response that does not coincide with the series resonance of L_2 and C_4. Varying the ratio of the series-resonant components, L_2 and C_4, will not change the overall RF transimpedance at the series resonant frequency, but it does contribute to the out-of-band peaking as shown in Figure 6

Figure 6, Transfer Function PD to RFout

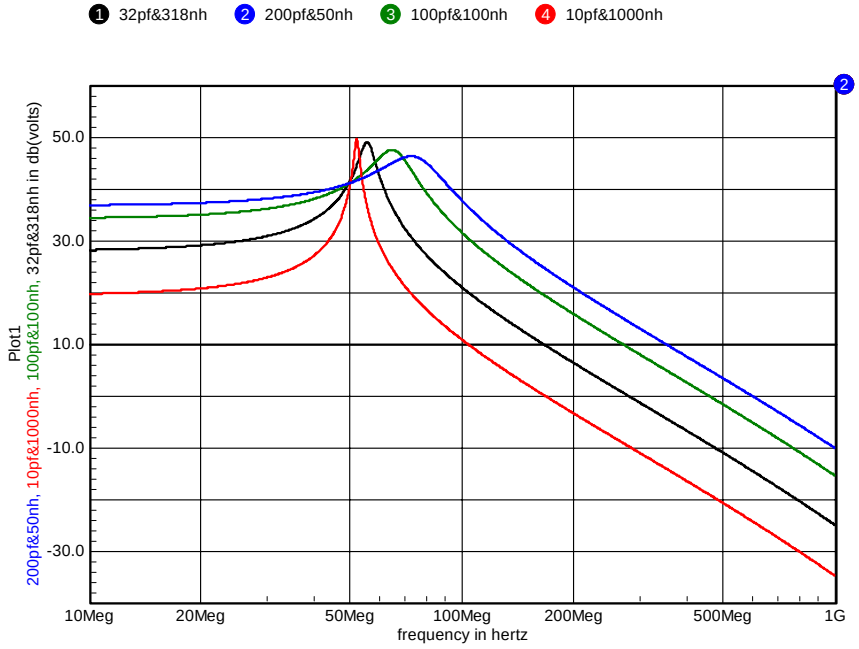

5.6. It is worth considering how one would tune such a detector to its operating frequency. The peak in the response no longer corresponds to the desired operating frequency. While tuning is possible, it would be seem less intuitive.

6. Variant 2

A second topology is presented in Figure 7 using an op-amp in a transimpedance configuration without presenting reactive components to the photo-diode.

Figure 7

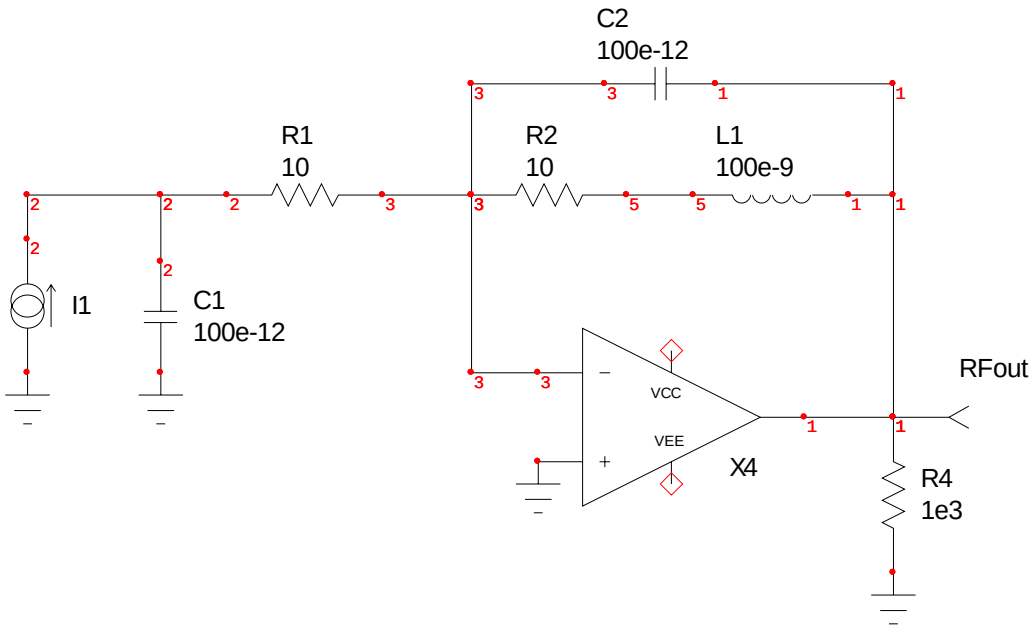

6.1. The signal voltage present at the RFout port associated with shot noise can be expressed by the component of the shot noise current flowing through R_1 multiplied by the transimpedance of X_4:

$$Vsignal_{RFout} = I_{shot} \cdot \frac{L_1}{C_2 \cdot R_2} \cdot \sqrt{\frac{1}{1+(\omega \cdot R_1 \cdot C_1)^2}}$$

R_2 is set at 10 Ω to provide 100 Ω transimpedance at 50 MHz

6.2. X_4 has an input impedance of <<1Ω provided the open loop gain is >>1 at the frequency of interest (50 MHz in this example). For a transimpedance of Z_t, the noise voltage at the output of X_4 is calculated as:

$$V_{noise} = \sqrt{(V_n)^2 + (I_n \cdot Z_t)^2}$$

6.3. The SNR for the standard set of conditions for Variant 2 is calculated to be:

SNR =5.97 (Identical to Variant 1)

6.4. Figure 8 shows a family of curves revealing the effect of different ratios of L_1 and C_2 while keeping a constant RF transimpedance by modifying R_2. In practice, higher RF transimpedances are usually welcome in sensitive applications, achieving lower values isn't difficult.

Figure 8

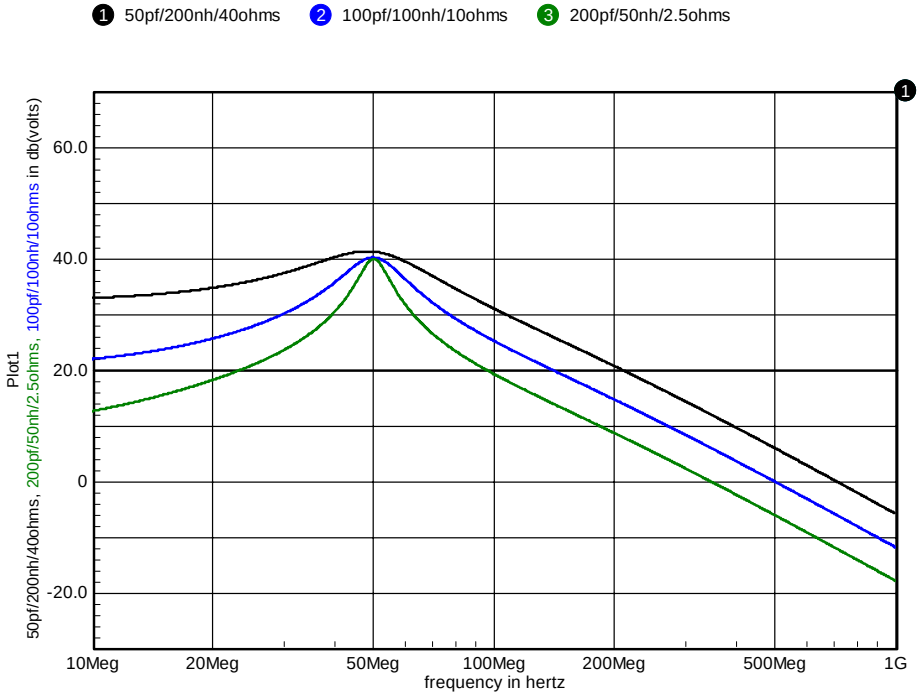

7. When considering the different topologies for RF photo-detector circuit design, additional parameters must be considered so as not to misinterpret the SNR results. The following section includes these factors and their impact on SNR.

7.1. Factors that influence topology selection

7.1.1. The manufacturing variations in photo-diode capacitance result in a need to re-tune photo-detectors that incorporate the photo-diode as part of a frequency-selective RF network. Designs that are insensitive to diode capacitance variations improve the mean-time-to-repair for a photo-detector.

7.1.2. RF photo-diodes are typically operated with a DC reverse-bias voltage to minimize the junction capacitance. Changes in the induced photo-current will cause variations in reverse-bias, thus coupling photo-current and junction capacitance. It is desirable to minimize this effect by choosing topologies wherein the RF tuning is insensitive to photo-diode capacitance.

7.1.3. It is often necessary to incorporate additional RF networks in parallel with the primary RF network. This is done to allow simultaneous extraction of different frequencies, or to reduce the effect of an undesired frequency

component. The ease with which these other networks can be implemented is a desirable characteristic. Certain topologies allow independent tuning of secondary filters without coupling to the primary resonance.

7.1.4. At LIGO, certain applications require a "canceling" signal to be injected into the resonant circuit of a photo-detector. This is done to reduce a parasitic signal that exists in quadrature to the desired signal using a system referred to as the "I-Phase Servo". The ease with which this injection can occur is a consideration in the choice of RF photo-detector topology.

7.2. Comparison Table

Table 1

Topology	**SNR For Standard Conditions**	**Diode Capacitance Insensitivity**	**Ease of Parallel RF Networks**	**I-Phase Servo Compatibility**	**Ease of Tuning**
Initial LIGO	**6.25:1** In practice this is hard to achieve with parallel networks	**Poor**. First order sensitivity	**Poor**. Can also reduce SNR	**Medium**	**Fair**. Typically needs tunable inductor
Sandberg et al.	**5.17:1** Compromised by voltage noise amplification	**Good**. Resonant circuit is independent of diode capacity	**Good**.	**Medium**	**Medium**. Parasitic resonances are present
Variant 1	**5.97:1** Improvement due to no amplification of voltage noise	**Good**. Resonant circuit is independent of diode capacity	**Good**.	**Good.** Can be done with single resistor into summing node	**Medium**. Parasitic resonances are present
Variant 2	**5.97:1** Improvement due to no amplification of voltage noise	**Good**. RF components isolated from diode capacitance	**Poor**. Hard to implement	**Good**. Can be done with single resistor into summing node	**Good**. Resonant circuit is well isolated from diode

8. Conclusions

8.1. Of the four topologies scrutinized by this analysis, there is no clear-cut favorite for all potential applications. It is also important to physically realize these designs, as many of the observations and conclusions are theoretical and potentially unrealizable. Variant 1 seems to provide the most promise prior to having hopes dashed by prototype results. Time will tell.

8.2. Experience gained during the operation of the initial LIGO detector has pointed to a need for more realizable designs that are easy to tune and repair. The rejection of unwanted signals was not to be undervalued, so future photo-detectors should strive to address these issues. Receiver design is always more simple when the only signals present are the ones you want.

8.3. Extraction and monitoring of the DC photo-current is generally needed. Some designs lend themselves to this task more efficiently than others. Prototyping is needed to properly weigh the results.